IEEE Access
Multidisciplinary | Rapid Review | Open Access Journal

Received April 21, 2021, accepted May 11, 2021, date of publication May 19, 2021, date of current version May 27, 2021.

Digital Object Identifier 10.1109/ACCESS.2021.3081680

A Joint Optimization Model for Energy and Reserve Capacity Scheduling With the Integration of Variable Energy Resources

M. WAJAHAT HASSAN[1], THAMER ALQUTHAMI[2], AHMAD H. MILYANI[2], ASHFAQ AHMAD[1], AND MUHAMMAD BABAR RASHEED[1,3], (Senior Member, IEEE)

[1]Department of Electronics and Electrical Systems, The University of Lahore, Lahore 54000, Pakistan
[2]Department of Electrical and Computer Engineering, King Abdulaziz University, Jeddah 21589, Saudi Arabia
[3]Department of Computer Engineering, University of Alcalá, 28805 Alcalá de Henares, Spain

Corresponding authors: Muhammad Babar Rasheed (muhammad.rasheed@uah.es) and Thamer Alquthami (tquthami@kau.edu.sa)

This work was supported in part by the Deanship of Scientific Research (DSR) at King Abdulaziz University, Jeddah, under Grant RG-13-135-41, and in part by the European Union Horizon 2020 Research and Innovation Program under the Marie Sklodowska-Curie Grant through GOT ENERGY TALENT under Agreement 754382.

ABSTRACT In this paper, a two-stage approach is proposed on a joint dispatch of thermal power generation and variable resources including a storage system. Although, the dispatch of alternate energy along with conventional resources has become increasingly important in the new utility environment. However, recent studies based on the uncertainty and worst-case scenario-oriented robust optimization methodology reveal the perplexities associated with renewable energy sources (RES). First, the load demand is predicted through a convolutional neural network (CNN) by taking the ISO-NECA hourly real-time data. Then, the joint dispatch of energy and spinning reserve capacity is performed with the integration of RES and battery storage system (BSS) to satisfy the predicted load demand. In addition, the generation system is penalized with a cost factor against load not served for the amount of energy demand which is not fulfilled due to generation constraints. Meanwhile, due to ramping of thermal units, the available surplus power will be stored in the backup energy storage system considering the state of charge of the storage system. The proposed method is applied on the IEEE-standard 6-Bus system and particle swarm optimization (PSO) algorithm is used to solve the cost minimization objective function. Finally, the proposed system performance has been verified along with the reliability during two worst-case scenarios, i.e., sudden drop in power demand and a short-fall at the generation end.

INDEX TERMS Co-dispatch, spinning reserve, state of charge, optimization, renewable energy resources, battery storage system, particle swarm optimization.

NOMENCLATURE

The main notations used in this paper are stated below. Additional symbols are defined in the article where required.

A. SETS AND INDICES

$n \in N$	Set of thermal generation units.
$k \in K$	Set of wind power units.
$l \in L$	Set of PV units.
$d \in D$	Set of loads.
$b \in B$	Set of nodes.
$u \in U$	Set of users.
$t \in T$	Index for time.

The associate editor coordinating the review of this manuscript and approving it for publication was Dwarkadas Pralhaddas Kothari.

B. DECISION VARIABLES

R_t	Reserve requirement at t^{th} hour [MW].
P_{nt}	Dispatch of thermal unit n over t^{th} hour [MW].
η_{nt}	Status of the n^{th} thermal unit over t^{th} hour.
P_{St}	Reserve capacity dispatch using BSS over t
C_t	Cost of power generation over the period t [$]
F_{nt}	Cost of n^{th} generation unit over t^{th} hour [$]
P_{kt}	Wind power output from unit k for t^{th} hour [MW].
P_{lt}	PV power output from unit l for t^{th} hour [MW].
$\overline{P_{u,t}}$	Max. demand of u^{th} user over t^{th} hour [MW].
$\underline{P_{u,t}}$	Min. demand of u^{th} user over t^{th} hour [MW].
$\widehat{P_{u,t}}$	Avg. power demand for u^{th} user over t^{th} hour [MW].
Φ_t	Expected energy not supplied for t^{th} hour [MW].

$\hat{G}_t$ Solar irradiance over the period t [W/m^2].
$\overline{G_t}$ Max. limit on solar irradiance over the period t [W/m^2].
$\underline{G_t}$ Min. limit on solar irradiance over the period t [W/m^2].

C. PARAMETERS

k^{VoLL} Penalty factor for expected energy not supplied.
Γ^{VoLL} Penalty factor incorporated in the case of loss of load.
$\underline{P_n}$ Min. limit on n^{th} thermal generation unit.
$\overline{P_n}$ Max. limit on n^{th} thermal generation unit.
$\lambda_n{}^{up}$ Ramp up rate of n^{th} thermal generation unit.
$\lambda_n{}^{dn}$ Ramp down rate of n^{th} thermal generation unit.
U_{nt} Status of n^{th} thermal generation unit at period t; 0 = OFF, 1 = ON.
C_{Q_n} Quadratic cost coefficient of n^{th} thermal generation unit.
C_{Ln} Linear cost coefficient of n^{th} thermal generation unit.
C_{Fn} Fixed cost coefficient of n^{th} thermal generation unit.
α_l Power temperature coefficient of l^{th} PV unit [$\%/C^\circ$].
v_{cut-in} Wind cut-in speed
$v_{cut-off}$ Wind cut-off speed
v_{rt} Rated wind speed
P_{st}^{+} Current power of storage unit during charging
P_{st}^{-} Current power of storage unit during discharging
$\overline{P_s^{+}}$ Max. power limit of storage unit during charging
$\underline{P_s^{+}}$ Min. power limit of storage unit during charging
$\overline{\overline{P_s^{-}}}$ Max. power limit of storage unit during discharging
$\underline{P_{st}^{-}}$ Max. power limit of storage unit during discharging
v_{d_s} Charging state of storage unit
v_{c_s} Discharging state of storage unit
v_{nt} ON/OFF state of generator n over time t
P_{nt} Power output of generator n over time t
$\overline{P_{nt}}$ Max. limit on current power of generator n over time t
$\underline{P_{nt}}$ Min. limit on current power of generator n over time t
E_{st}^{+} Energy storage level during charging.
E_{st}^{-} Energy storage level during discharging.
γ_{st} Power available for storage over time t.
γ_s Capacity of BSS.
σ_s State of charge.
σ_{s_0} State of charge at zeroth hour.
$\overline{E_s}$ Max. limit on energy storage
$\underline{E_s}$ Min. limit on energy storage
η_s Battery power losses

I. INTRODUCTION

The electrical system operator (ESO) is responsible to generate the power and he has to face plentiful multifaceted perplexities to make the system work fluently. Generally, the power system consists of heterogeneous devices with diverse operating parameters (refer to figure 1). The system is consistently prone to get more complicated through the integration of linear and non-linear load, communication devices, smart metering, distributed storage systems, security and quality improvement. These complexities get increased when the lifestyle of individuals is improved and the system is made more sustainable. ESO has to take the responsibility to foresee each and every aspect of the smooth and less-vulnerable operation of the electricity market. Furthermore, the ESO can handle this situation by making the adjustments on generation side and hence providing the price based DR programs to balance the generation-demand during peak hours [1]–[4]. The activity of appliances on the user end are restrained in response to the dynamic price being offered to reduce the electricity cost without affecting the comfort level [5]–[9]. However, at the consumer side, there is a need to make it mandatory to automate the accurate appliance switching with respect to dynamic pricing. For this purpose, direct load control models are implemented [10], [11]. On the broader view, the electricity market has gone a rapid transformation with the involvement of smart grids (SG) [12], [13]. The technology advancements, evolving consumer preferences, and new policies are leading to a surge of penetration of renewable energy sources (RES), BSS, microgrids, electric vehicles, and other new energy technologies. The RES penetration is environment friendly, however, it involves the variations in power generation due to their dependency over natural phenomena [14]. Such kind of versatile and distributed energy generation systems are propelling the utility and regulating bodies to reassess "how the electricity market performs in agreeable manner". Therefore, the new models for customer energy management, grid infrastructure and electricity market design are required to address these changes.

While the electric power demand and the price of electricity are the most influential factors in the electricity market. Therefore, the system quality, control, reliability and management of electricity market operations, are essential to have an accurate assessment of the day ahead power demand. Because the electricity selling/buying contracts are based on the price being offered by the cost of generation and the transmission and distribution infrastructure. While the exact approximation of the load demand and price through forecasting methods enables the market shareholders to make the most productive and pragmatic bidding strategies [15]–[18]. On the other hand, the penetration of RES in a power system comes with inherent uncertainty due to uncertain generated power. Thus, the unpredictability due to availability of sunlight in the case of photovoltaic (PV) while the wind power is substantially effected due to variations in the wind speed. The issue of uncertainties in the RES output is explored

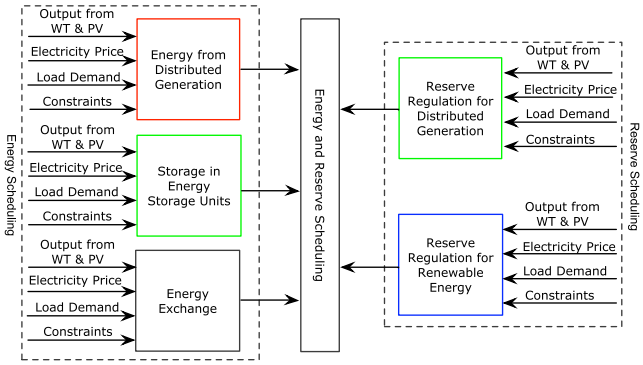

FIGURE 1. Overview of an electricity market.

widely and addressed with various robust optimization methods, where these methods involve probability distribution and computation with mathematical approximations as in [19].

A. REAL CONTRIBUTIONS

This paper proposes a system model of joint dispatch of energy and reserve capacity with the integration of RES and BSS. The load demand has been forecasted using (CNN) for a certain area where the system is considered to be implemented. The power demand is fulfilled through liquid fuel thermal generation units (LFTGU), RES and BSS in such a way to reduce the possible cost. The expected energy not supplied (EENS) is measured where the actual demand becomes more than the forecasted value the spinning reserve is not enough to cope up with this change or the system has encountered any collapse in the power generation from the expected value. EENS is treated as a system penalty cost as a value of lost load (VoLL) which is taken as a constant value constrained within some operational limits [20]. The thermal power generation cost calculated while ramping and committed/shutdown states are taken into consideration. The BSS is incorporated to store surplus generated power and can be made available as the reserve capacity. The PSO is used to get cost minimized results in the dispatch of generated power. For a detailed analysis the following test cases are implemented.

1) CASE 1

In the 6-Bus system under consideration, which is performing in steady state, it is assumed that there is a sudden decline in power demand due to fault at a supply line connecting 2 buses. The LFTGUs bears some excessive production of spinning reserve capacity due to ramping. The troubles created by this unforeseen fault are studied in this scenario.

2) CASE 2

After undergoing the sudden loss in the power demand, the system is thought to encounter another mess, i.e., one of the generation units is gone off-line. The effects of this loss propagate in the hours coming soon after. The unit is supposed to be on-line in the very next hour, but due to ramping it must increase its output power gradually.

The rest of paper is structured as follows. Section II presents the detailed literature review which gave motivational ideas. The relevant formulations and algorithm details are given in Section III. Case studies to validate the proposed models are presented along with their results in Section IV. Finally, the conclusion is drawn in Section V.

II. MOTIVATION AND BACKGROUND LITERATURE

In the long-term planning for the design of electrical system and electricity market, there are a lot of challenges one has to come up with. Both the ESO and consumer want to get maximum benefit from the system in the sense of profit or user comfort. This could only be possible when the system works with reliability and effective style. On the ESO side, the main problem is the scheduling of generated power to settle the demand. For this purpose, the ESO must investigate the power demand in the electricity market ahead of the real time to commit the available power on the generation side. Previous statistics of power demand for hourly, daily and yearly bases along with weather prediction data is taken as decisive features for day-ahead load forecasting. While the neural network techniques (NN) and deep learning (DL) based frameworks are required to assess the upcoming load demand. These methods take weather, time and socio economic data to facilitate the decision making algorithms. The predicted measure of load demand requires a cost optimal dispatch of energy. In [21]–[24], the authors have shown that the load forecasting techniques, in a large area by clustering the electricity consumers on the basis of their behaviour, have produced efficient results. To settle the load demand the power is granted by set of sources including the LFTGU, RES, and BSS. This mixture of resources has triggered the areas of research and development, regarding how the power generation is managed, controlled and scheduled. However, due to uncertain availability of RES and variations on generation side caused by them, there is a need for increased amount of operational flexibility in the system. The ESO could offer ancillary services to achieve a more robust operation of the system and also improve their profit. Therefore, in this regard some studies have quantified the provision of reserve energy as given in [25]–[30]. These studies have focused solely on optimizing the economic operation of the combined dispatch of energy and reserve [31].

Considering the LFTGUs, the output power from on-line units is constrained within their minimum and maximum generation limits, prohibited zones and ramping. The ramp rate or power response rate can be explained as a response capability of the thermal unit in terms of changing power variations in specified time interval. Figure 3 shows three possible working scenarios if an on-line LFTGU is operated from $(t-1)^{th}$ hour to t^{th} hour. In figure 3a the thermal unit provides constant power through time considered. Figure 3b shows that the power is increased as compared to previous hour and figure 3c shows decreasing power generation status. This increment or decrement of the power in a time is constrained within the ramp-rate limits. The thermal unit can increase it

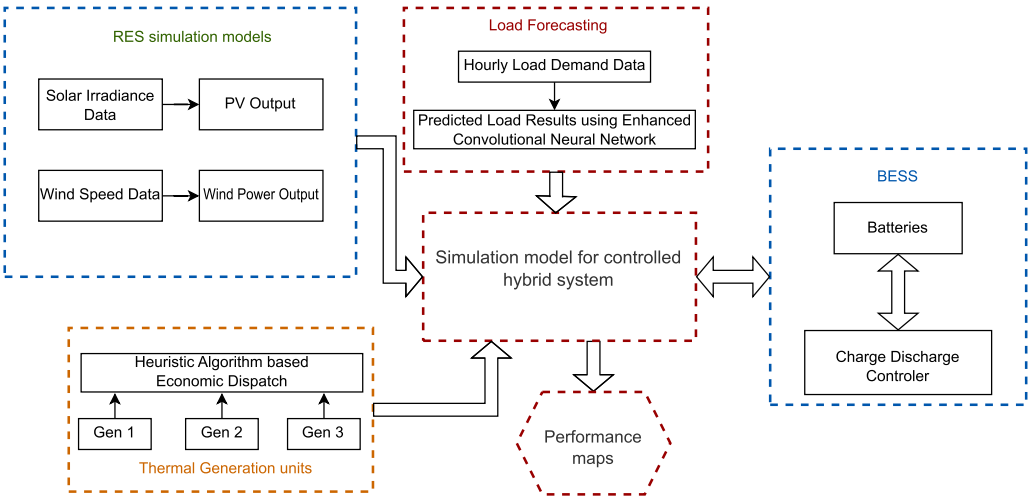

FIGURE 2. Proposed model and control methodology.

generation to a certain extent in given time remaining within its maximum limits and, conversely it can decrease its power to the ramp limits. Moreover, once a thermal unit is gone off due to diminishing load demand, it will require some time to be on-line; i.e., become the part of generation, because of cooling down and again heating up the boiler, so there is a start-up time lapse. This can also cause the curtailment in generation.

On the other hand, the RES integration is major part of recent modernization in the electrical power system. To achieve this enhancement in the system, mathematical models of PV and wind power plants are implemented as given in [32]. The output of these mathematical models is taken as a share in energy generation and, therefore given superiority as being the low cost and environment friendly mode of harnessing electrical power. The mathematical models relate the natural resources with the electrical power output of the generator. Although, there is a vast range of RES technologies, however, in this research only PV and wind technologies are taken into consideration. To improve the reliability of the system, the backup storage has now become vital part of the system. Due to the increased number of electric vehicles (EV) and their charging stations, EVs can provide a storage facility in the system for a duration of minutes up to several hours. The authors, in [33]–[36] has discussed the methods EVs can be connected in the system, in a way of the vehicle to grid (V2G) and grid to the vehicle (G2V) energy transfer. As they can provide constant and immediate alternate power source to grid. Moreover, presuming that the main power is out or running short of the required demand BSS can play its part as an energy buffer the daily load balancing. In this research, BSS is incorporated as a spinning reserve facility. The storage status is expressed in terms of state of charge (SoC) for batteries. Due to the ramping in the nature of thermal units, the generated power cannot be diminished abruptly with the load being reduced suddenly. This surplus generated power is used to raise SoC whenever available. At times, the sudden increase in the demand, or loss of thermal generation or RES, the BSS will be used to settle the demand while SoC will decrease. The simulation model of BSS is used to get the SoC levels while taking and storing the energy into the BSS. Such simulations models are given in [37]–[39] with optimum allocation of BSS and charge/discharge control mechanisms. After the detailed reviewing of recent literature, the following points discuss the motivations of this work:

- The exploitation of the combined dispatch of thermal, PV, and storage plants is getting attention nowadays as previously explained in [20] and [21]. This is due to the overuse of conventional energy sources concerns has been raised over its global climatic and economic effects. As a result, the exploration in the field of clean and green energy and the strive to improve their efficiency has become increased.
- For stable and efficient energy management, generators scheduling, and power dispatch the forecasting of power demand is of crucial importance. Operations in power systems rely heavily on precise forecasting of future loads on various time horizons. An intelligent data-driven neural network methodology can be applied to assess short-term load forecasting.
- Thermal generation capacity can be optimized for the minimum cost, using bio-inspired algorithms. As the thermal generation undergoes some natural phenomenon, i.e., ramping nature of thermal units, therefore, this makes the system vulnerable to some unforeseen changes in the system power, such as sudden drop or increase in the load demand in the system.
- To make the power system more reliable against such variations, a storage system must be provided to contribute a cushion in the power demand and supply.

The recent literature has provided enough directions to make the system more reliable, we have combined all of the major concepts proposed individually in the cited papers i.e, load

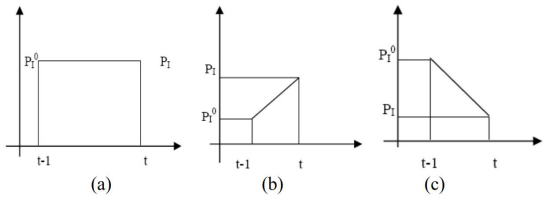

FIGURE 3. Three possible situations of power output for an on-line LFTGU.

forecasting to dispatch of generation along with reserve using a heuristic algorithm, incorporation of uncertain RES to the provision of a spinning reserve through BSS. Furthermore, the discussion and analysis in this paper extend the preliminary results in our earlier paper [31] in various aspects. First, here we have implemented the load forecasting technique instead of taking arbitrary load demand. Second, we are taking BSS to incorporate the spinning reserve in the system. Finally, the two worst-case scenarios are structured and the energy dispatch results are simulated in a way to demonstrate the efficiency and reliability of the system. The results and discussion include the detailed analysis of the test cases implemented to have a better understanding of the provisioning of spinning reserve and highlight the impact of a sudden loss of load occurred at any instance.

III. MATHEMATICAL MODELS

Mathematical formulation starts with the assessment of load demand in the system.

A. LOAD FORECASTING USING NN

This is done using convolutional neural network (CNN) which is DL technique based on supervised learning famously used for prediction. The CNN inspired by biological processes, use relatively less pre-processing than other classification algorithms i.e. it learns the filters that used to be hand engineered in traditional algorithms [40]. To improve the efficiency and speed of the algorithm the selective features are refined.

The flow of this algorithm is shown in figure 4. The CNN model applied to get the best forecasted results of load demand, deals efficiently with the hourly load demand data of a certain region for a complete year. The simulation results show that accuracy of the algorithm.

The modeling of cost minimization for electric power system at the generation end starts with the formulation of unit commitment problem.

B. UNIT COMMITMENT

This section gives a basic understanding of unit commitment modeling. The thermal generation units are committed according to the predicted load. If an on-line generator is not contributing to the load, it will cause fixed cost of running the unit. If the load prediction is to be on lower side for a longer time and can be settled without high cost unit, that unit will not be committed to the system and will go off-line to save

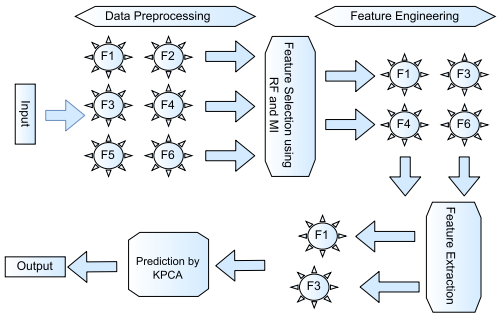

FIGURE 4. Flowchart of CNN.

the fixed cost. The unit commitment problem given the status of all generating units to be in the binary form, i.e., ON/OFF. The units committed to provide power for the settlement of demand, are then applied the economic dispatch technique, to find the best generation value for each generator in the lowest cost. The mathematical equation of this minimization problem is given below:

$$\min. \sum_{n=1}^{N} \sum_{t=1}^{T} C\left(\eta_{nt}, P_{nt}\right) \quad \forall n \in N. \tag{1}$$

The eq. 1, is the mathematical model of the cost optimization problem. The C is the generation cost, which is the function of η_{nt} and P_{nt}. Where, η_{nt} is the binary status of n^{th} generation unit, which tells the availibility of it during any period t and P_{nt} is the output power of n^{th} LFTGU over the period t.

1) PV

The mathematical model presented in [32] is used for PV power calculations. The output power of a PV panel is calculated using equation (2) and is given below:

$$P_{l_t} = P_l{}^{STC}\left\{\frac{\hat{G}_t}{1000}\left[1+\sigma_l\left(T_{cell,t}-25\right)\right]\right\} \quad \forall l \in L. \tag{2}$$

The Progensa's PV model presented in the eq. 2 is used to caluclate the output of PV generation. In this mathematical model, the $P_l{}^{STC}$ is the output power of l^{th} PV unit on standard test conditions, σ_l is the power-temperature coefficient of l^{th} PV unit taken as $\%/^{\circ}C$, which tells the percentage change in the output power with a change of 1°C in the cell temperature. Moreover, the G_t is the average value taken of solar irradiance in W/m^2 over the period t which is calculated hourly using eq. 3.

$$\hat{G}_t = \frac{\left(\overline{G_t} + \underline{G_t}\right)}{2} \quad \forall t \in T. \tag{3}$$

Average solar irradiance is calculated by taking the mean of maximum $\overline{G_t}$ and minimum $\underline{G_t}$ solar irradiance occured over the period t.

The dataset for a typical 24 hours duration is taken and given in the table 2. $P_l{}^{STC}$ of the PV generation is taken to be 30MW. The data about a single module of PV is given in the table 4.

2) WIND

The mathematical model presented in [32] is used for the wind power calculations. The output power of a wind power plant is dependent on the wind speed, which keeps varying due to natural behaviour. The model of wind power incorporates alternating nature of the wind speed and gives output in discrete mathematical form as given in equation below;

$$P_{kt} = \begin{cases} 0; & v_t < v_{cut-in} \\ \frac{P_{k,rt}}{v_{rt}-v_{cut-in}} v_t + \\ P_{k,rt}\left(1 - \frac{v_{rt}}{v_{rt}-v_{cut-in}}\right); & \\ & v_{cut-in} < v_t < v_{rt} \\ P_{k,rt}; & v_{rt} < v_t < v_{cut-off} \\ 0; & v_t > v_{cut-off} \end{cases} \quad \forall\ k \in K$$

This tells about the output of the wind power. While the output depends only on the wind speed, if the wind speed being less than the minimum value v_{cut-in} or greater than the maximum value $v_{cut-off}$ the output stays zero, i.e. electricity cannot be generated with lesser wind speed, however, the wind blades can face damage with more speed so the wind plant has to be shut-off. The wind output is only available if the wind speed is in-between these parameters, while it will be equal to rated power when wind speed is above v_{rt},. i.e. rated speed. The dataset for a typical 24 hours duration is taken and given in the table 3. Where P_{rt} is the combined rated output of the wind generation from all wind power units. Which is taken to be 10MW, and other quantities about a single wind turbine are mentioned in the table 4.

C. CO-DISPATCH USING RAMP RATES AND EENS

The cost of generation is raised considering the penalty factor as (k^{VoLL}) when the system is not capable of supplying the complete demand. Penalty factor has been taken with an arbitrary value of 100$ per MW of the power not supplied.

$$\min. \sum_{n=1}^{N}\sum_{t=1}^{T}\left(C\left(\eta_{n_t}, P_{nt}\right) + (k_{nt}^{VoLL} * \Phi_t)\right) \tag{4}$$

The objective function of the proposed cost minimization model is given in eq. 4. This is a dual minimization problem, in which generation cost along with the value of the lost load is jointly minimized. The Φ_t is the amount of EENS for the period t, it is multiplied by a factor to find the value of the lost load.

$$\Phi_t = \sum_{d=1}^{D}\left(P_{d_t}\right) - \left(\sum_{n=1}^{N}\left(P_{n_t}\right) + \sum_{k=1}^{K}\left(P_{k_t}\right) + \sum_{l=1}^{L}\left(P_{l_t}\right) + P_{S_t}\right) \tag{5}$$

The eq. 5 given the mathematical explanation on how Φ_t is calculated, as the difference between the load demand and the total available generation, i.e., RES, LFTGUs, and reserve.

The load demand $\left(P_{d_t}\right)$ occurred over an hour t can be calculated by taking sum of all the load occured at system by (U) users. Its mathematical form is given in eq. 6:

$$P_{d_t} = \sum_{u=1}^{U} \hat{P_{ut}} \quad \forall u \in U,\ t \in T. \tag{6}$$

The average load demand $\hat{P_{ut}}$ over an hour t can be calculated by taking the mean value of maximum load $(\overline{P_{u,t}})$ and minimum load $(\underline{P_{u,t}})$ for that hour as given in eq. 7:

$$\hat{P_{ut}} = \frac{\left(\overline{P_{u,t}} + \underline{P_{u,t}}\right)}{2} \quad \forall u \in U,\ t \in T. \tag{7}$$

And the quadratic cost function of each thermal unit over t is given by the eq. 8;

$$F_{nt} = C_{Q_n} {P_{nt}}^2 + C_{Ln} P_{nt} + C_{Fn} \quad \forall\ n \in N. \tag{8}$$

The eq. 8 is a generic cost function of a thermal generator. C_{Q_n} is the quadratic coefficient of cost, C_{Ln} is the linear coefficient of the cost, and C_{Fn} is the fixed cost of n^{th} unit. F_{nt} is the cost of n^{th} unit over period t obtained at any output power P.

This optimization problem is constrained with operational limits as load/generation balance, and the generation unit limits that are explained as below:

1) CAPACITY LIMITS

All committed LFTGUs can operate withing their operational limits and the generated power must always be positive. Eq. 9 denotes the upper and lower limit on the dispatch power of all the units and eq. 10 shows that at any time t, the generation must always be greater than zero.

$$\underline{P_n} \le P_{nt} \le \overline{P_n}, \quad \forall n \in N,\ t \in T. \tag{9}$$

$$0 \le P_{nt}, \quad \forall n \in N,\ t \in T. \tag{10}$$

2) EENS

The total demand is fulfilled using power generated from thermal units, RES and BSS respectively. While, the load demand is not fully satisfied the EENS limit will be incorporated. As given in eq. 5.

3) RAMP RATE LIMIT CONSTRAINT

Furthermore, the P_{nt} by the n^{th} LFTGU over interval t may not exceed that of previous interval $(t-1)$ by more than a certain amount ${\lambda_n}^{up}$, which is the up-ramp rate. On the other hand, it cannot be less than that of the previous interval by more than some amount ${\lambda_n}^{dn}$, which is the down-ramp rate limit of the generator. These give rise to the following constraints: eqs. 11 and 12:

$$P_{nt} \le \max\{\overline{P_n}, (P_{n(t-1)} + {\lambda_n}^{up})\}, \quad \forall n \in N,\ t \in T. \tag{11}$$

$$\min\{\underline{P_n}, P_{n(t-1)} - {\lambda_n}^{dn}\} \le P_{nt}, \quad \forall n \in N,\ t \in T. \tag{12}$$

where, ${\lambda_n}^{up}$ and ${\lambda_n}^{dn}$ are the ramp-up and ramp-down rates for n^{th} thermal generation unit.

$$v_{nt} + v_{nt-1} - \mu_{nt} = u_{nt}, \quad \forall n \in N,\ t \in T \tag{13}$$

TABLE 1. Operating limits and cost coefficients of generation units [31].

Gen	P_{min}[MW]	P_{max}[MW]	C_{Q_n}	C_{Ln}	C_{Fn}	${\Lambda_n}^{down}$ [MW]	${\Lambda_n}^{up}$ [MW]
1	50	200	1.07e-2	1.1699e+1	213	30	30
2	37.5	150	1.78e-2	1.0333e+1	200	20	20
3	45	180	1.48e-2	1.033e+1	240	40	40

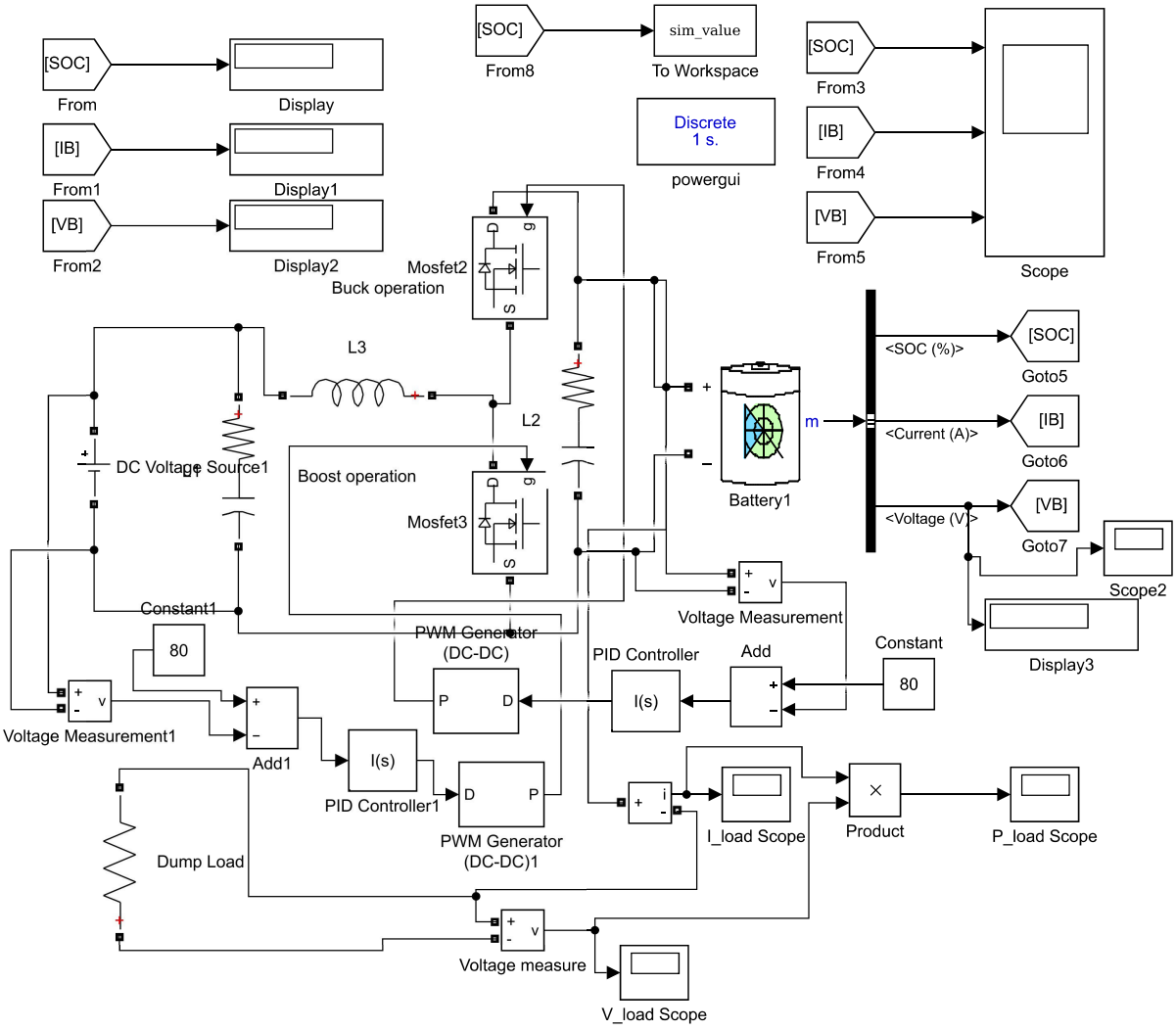

FIGURE 5. Simulink model of BSS with DC-DC charge discharge controller.

$$v_{nt} + \mu_{nt} \leq 1, \quad \forall n \in N,\ t \in T \tag{14}$$

Eq. 13 describes the state equations of dispatchable generators showing ON/OFF states. Where, v_{nt} is the ON/OFF state and μ_{nt} shows the shutdown state of dispatchable generators, respectively. Eq. 14 shows that these dispatchable generators cannot start and shut-down, simultaneously. The generator data has been taken from the IEEE standard bus system as mentioned in the table 1.

D. BSS MODEL

Batteries are incorporated to add autonomy in the system by providing energy storage which is generated in excess to the demand, i.e., due to the ramping in the LFTGUs. In this work, the sizing of the battery bank is done which ensures the autonomy of the system for 2 hours for the average consumption of users in the area under consideration.

$$\gamma_{st} = \sum_{t=1}^{T}(\sum_{n=1}^{N} P_{nt} - \Phi_t), \quad \forall n \in N,\ t \in T \tag{15}$$

$$v_{nt}\underline{P_n} \leq P_{nt} \leq v_{nt}\overline{P_n}, \quad \forall n \in N,\ t \in T \tag{16}$$

$$v_{cst}\underline{P_s^+} \leq P_{st}^+ \leq v_{cst}\overline{P_s^+}, \quad \forall n \in N,\ t \in T \tag{17}$$

$$v_{dst}\underline{P_s^-} \leq P_{st}^- \leq v_{dst}\overline{P_s^-}, \quad \forall n \in N,\ t \in T \tag{18}$$

Eq. 15 refers to the available surplus energy for BSS, where, Φ_t defines the expected amount of energy not supplied

TABLE 2. 24 hours dataset taken for PV.

Time (HRS)	12AM	1AM	2AM	3AM	4AM	5AM
G (Watts/m^2)	0	0	0	0	0	0
T_{cell} (MWatts)	25	22	26	28	22	30
Time (HRS)	6AM	7AM	8AM	9AM	10AM	11AM
G (Watts/m^2)	0	0	58	317	685	738
T_{cell} (C^o)	38	32	30	30	31	32
Time (HRS)	12PM	1PM	2PM	3PM	4PM	5PM
G (Watts/m^2)	705	784	619	530	256	66
T_{cell} (C^o)	33	34	31	35	30	30
Time (HRS)	6PM	7PM	8PM	9PM	10PM	11PM
G (Watts/m^2)	0	0	0	0	0	0
T_{cell} (C^o)	24	23	28	20	24	25

TABLE 3. 24 hours dataset taken for wind.

Time (HRS)	12AM	1AM	2AM	3AM	4AM	5AM
v (m/sec)	23	11	42	9	34	24
Time (HRS)	6AM	7AM	8AM	9AM	10AM	11AM
v(m/sec)	14	37	20	8	13	11
Time (HRS)	12PM	1PM	2PM	3PM	4PM	5PM
v (m/sec)	18	31	41	34	13	9
Time (HRS)	6PM	7PM	8PM	9PM	10PM	11PM
v (m/sec)	12	41	42	6	29	23

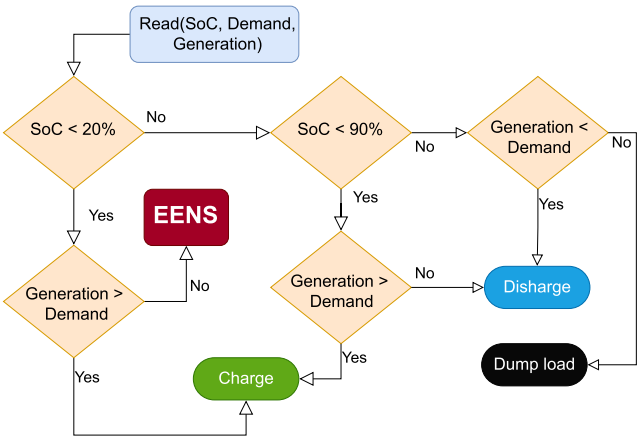

FIGURE 6. BSS control strategy.

during time t, P_{nt} is the dispatched power, γ_{st} is the remaining amount of power available for storage system. Eq. 16 defines the BSS power capacity limit. While eqs. 17 and 18 define charging and discharging limits on energy storage units, respectively. Where, v_{cst} and v_{dst} define charging and discharging states, and P_{st} is the power of the storage units.

$$\underline{E_s} \leq E_{st}^{+} \leq \overline{E_s} \tag{19}$$

$$\underline{E_s} \leq E_{st}^{-} \leq \overline{E_s} \tag{20}$$

Eq. 19 and 20 describe the capacity constraints on energy storage units during charging and discharging states, and $\overline{E_s}$ and $\underline{E_s}$ denotes the maximum and minimum storage levels respectively. However, E_{st} is the amount of energy stored over the period t.

$$E_{st} = E_{s_{t-1}} + \eta_s(E_{st}^{-} + E_{st}^{+}) \tag{21}$$

Eq. 21 presents the storage state equation on these units. Where, η_s is the power loss during charging and discharging

TABLE 4. Data of RES and BSS modules [44].

PV module		Wind turbine		BSS	
Sharp -ND-Serie A5		Angel Wind Energy - ProvenEnergy		Lg chem - BAT - 2.0 - A- SE-10	
Pmax (W)	250	Pmax (kW)	2.5	Energy capacity (kWh)	2
Isc(A)	8.68	v_{rt} (m/s)	30	Charging efficiency (%)	98
Voc(V)	37.6	Hub hright (m)	14.5		
Impp(A)	8.1	Turbine power loss (%)	6		
Vmpp(V)	30.9	Rotor diameter (m)	3.5		
Cell Area (cm^2)	156.5	v_{cut-in}	15		
Cells wired in series	60	$v_{cut-off}$	40		
α_l (%°/C)	2				

process, E_{st}^{+} denotes the energy storage level during charging and E_{st}^{-} denotes the energy storage level during discharging.

$$\text{when t} = 0 \quad E_{st} = \sigma_{(s_0)}, \quad \forall t \in T \tag{22}$$

Eq. 22 defines initial energy storage state and s_0 denotes zero state and so on.

$$0 \leq (v_{cst} + v_{cst-1}) + v_{dst} \leq 1 \tag{23}$$

Eq. 23 is charging and discharging rule such that charging and discharging cannot be done, simultaneously. The battery storage model is implemented in the Simulink. The battery bank is associated to the proposed system through a bi-directional DC/DC converter. While determining the appropriate size of BSS for a particular application, one generally selects the size based on the period for which load is expected to be supported over BSS [41], [42]. To retain high conversion efficiency and large backup storage a battery bank is produced by connecting adequate batteries in series/parallel arrays. However, this makes it necessary to have a battery management system with charge equalization for all serial arrays [43]. In this work, the battery bank consisting of a single module as given in the table 4 and the number of modules assumed to be of large capacity to store enough surplus power in the system, i.e., 25% of the average predicted load demand.

At the start of simulation, the BSS is assumed not to be fully drained. The SOC of BSS at the zeroth hour i.e., σ_{s_0} is taken to be 50%. Furthermore, the control strategy in the BSS will make sure that the BSS operate within the range of 20%-90% SoC levels. If the generation is not enough to settle the demand and while the SoC level falls below 20% then the power supplied from BSS will shut off to avoid the full discharge. Discharging of BSS is expressed in terms of decreasing SOC as given in eq. 24.

$$\sigma_{s_{t+1}} = \frac{\sigma_s \underline{P_s^{-}} - \gamma_{st}}{\gamma_s} \quad \forall \gamma_{st} < 0 \tag{24}$$

During discharge, where surplus power is calculated to be negative, the SOC for that hour is caluclated by taking

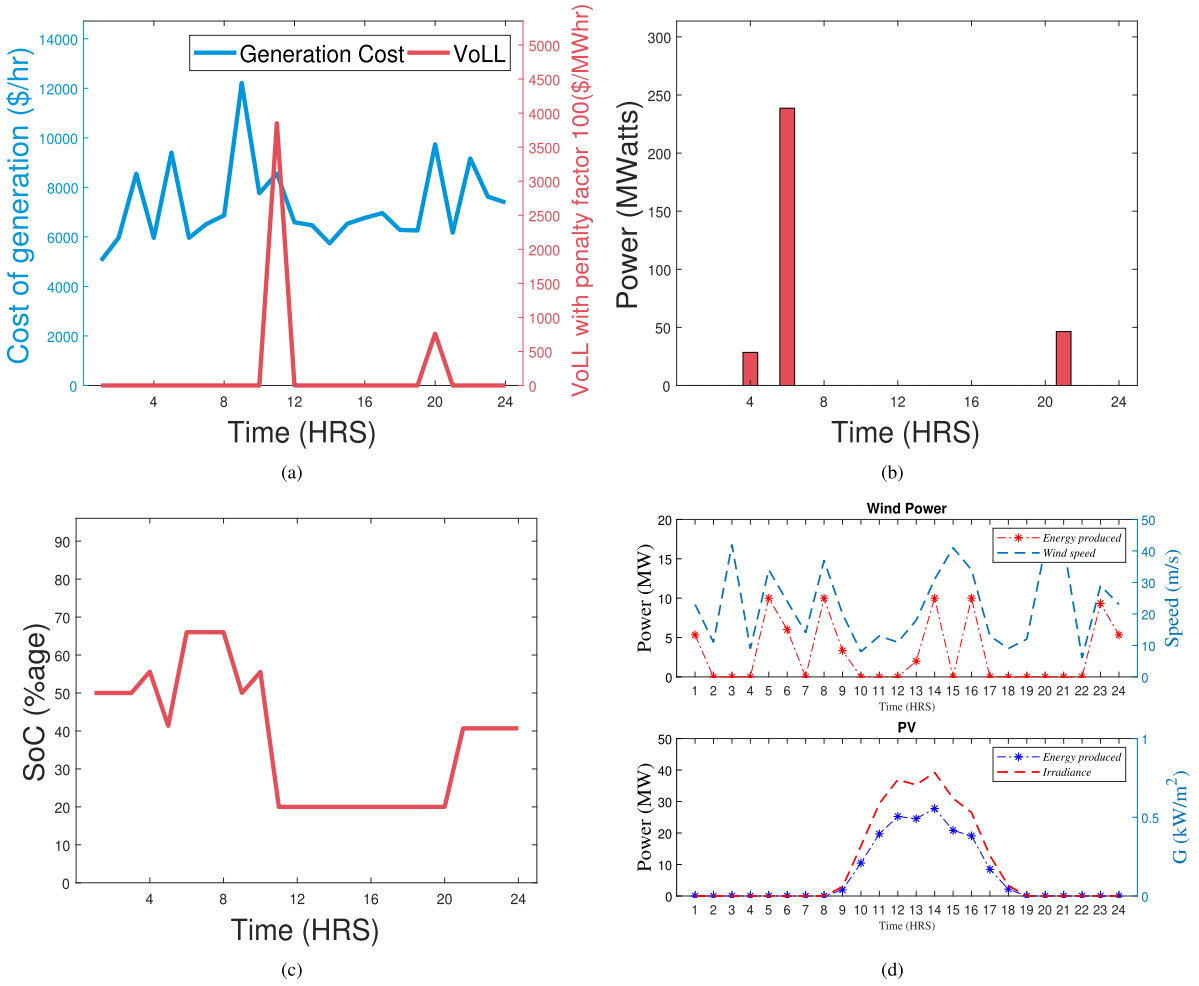

FIGURE 7. (a) Total cost of generation, (b) SOC of BSS plotted for 24h as a percentage of total charge level, (c) Surplus power available for battery storage, (d) Renewable power generated from Wind and PV.

difference of stored energy and γ_{st}, and then dividing the balance with BSS minimum capacity. Meanwhile, the load will not be served and EENS will take place, until the LFTGUs ramp-up their power to feed the load and charge the BSS as well. During the hour, in which the demand is cut-short compared with total available generation i.e., RES and LFTGUs, and the surplus power will be stored, until the SoC level reaches to 90%. In the case of SoC level reaches above 90% the dump load will be connected in the system to avoid overcharging and prevent bus voltage increasing. Charging of BSS is expressed in terms of increasing SOC as given in eq. 25.

$$\sigma_{s_{t+1}} = \frac{\sigma_s \overline{P_s^+} + \gamma_{st}}{\gamma_s} \quad \forall \gamma_{st} > 0 \tag{25}$$

During charge, where surplus power is calculated to be positive, the SOC for that hour is caluclated by adding the stored energy and γ_{st}, and then dividing the balance with BSS maximum capacity.

At any time, the SOC is subjected to minimum and maximum allowable SOC given in Eqs. 17 and 18. Moreover, the BSS control strategy is presented in the figure 6.

Figure 5 presents the proposed DC-DC charge controller with BSS which is connected to our system. The scope is used to display battery performance parameters, i.e., SoC, battery current and battery terminal voltage. This block is modeled as a function, which is called in Matlab code. The parameters sent to the Simulink model are the surplus power to be stored in the BSS. The Simulink model performs the simulation as per design and stores the power as per the received value from the MATLAB function. After this simulation is completed, the updated values of SOC (σ_s) are returned to the calling function. On the other hand, when power generation remains on the lesser side the load is fed through BSS.

IV. OPTIMIZATION MODEL

Particle swarm optimization with modified evaluation function is proposed in this research for the economic dispatch results. Various constraints such as generator limits, generator ramp rates, and losses are taken into account. The load demand is satisfied first by the RES available, the remaining demand is then dispatched by generation from LFTGUs with optimized power generation cost. PSO uses a vectorized search space where each particle in the search space presents

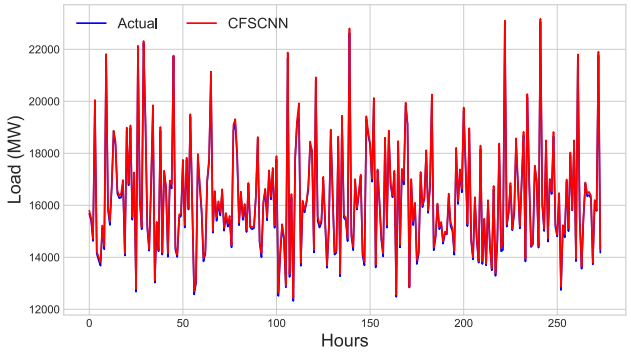

FIGURE 8. Load forecasting results compared with testing values.

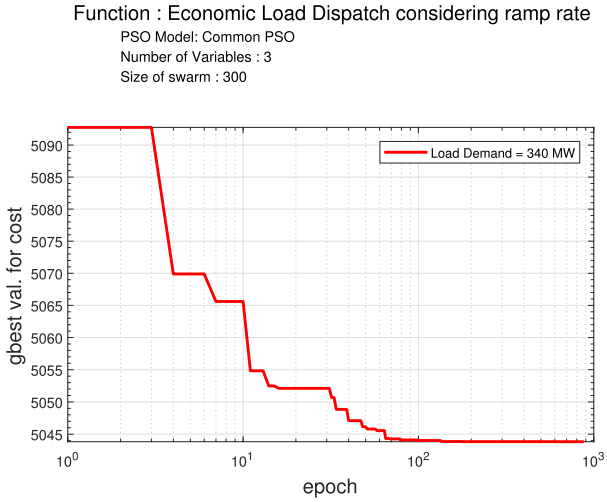

FIGURE 9. PSO based Economic Load Dispatch, convergence plot shown for the hour 1 with first 1000 iterations.

a solution. As shown in eq. 26.

$$\text{particle} \quad x_m^k = [P_1 \quad P_2 \quad P_3 \quad \dots \quad P_n] \tag{26}$$

The eq. 26 refers to the generation of population of n particles.

$$v_{m,n}^{k+1,P} = w\left(v_{m,n}^{k,P}\right) + d_1\rho_1\left(\epsilon_{m,n}^{P} - x_{m,t}^{k+1,P}\right) + d_2\rho_2\left(\varrho_{m,n}^{P} - x_{m,t}^{k+1,P}\right) \tag{27}$$

The eq. 27 gives detail how the velocity of each particle is calculated in $(k+1)^{th}$ iteration.

$$x_{m,n}^{k+1,P} = x_{m,n}^{k,P} + v_{m,t}^{k+1,P} \tag{28}$$

The position of each particle can be found using the eq. 28 for $(k+1)^{th}$ iteration.

The velocity and inertia for each particle in an iteration is bounded with in following limits:

$$v^{P,min} \leq v_m^k \leq v^{P,max}$$
$$\omega^{P,min} \leq \omega_m^k \leq \omega^{P,max}$$

$x_{m,n}^{k,P}$: It represents P_n;
v_m^k: velocity at k^{th} iteration for particle m;
$v^{P,max}$: max. velocity for particle m;

TABLE 5. Dispatch results for 24 hours.

Hours	Demand [MW]	P1	P2	P3	Losses	Cost[$]
1	340.0	110.6	106.1	135.3	12.0	5043.8
2	409.0	136.3	122.2	157.3	16.8	5967.0
3	490.0	166.3	142.2	180.0	23.3	8551.2
4	374.0	136.3	122.4	156.6	16.8	5959.1
5	510.0	166.3	142.4	180.0	23.4	9406.6
6	160.0	136.3	122.7	156.5	16.8	5962.0
7	443.0	151.1	131.9	170.1	20.0	6522.4
8	457.0	160.3	137.7	177.8	22.1	6868.5
9	405.0	190.3	150.0	0.0	16.4	12221.0
10	439.0	199.5	146.3	44.9	19.3	7735.2
11	515.0	200.0	150.0	84.9	25.5	8565.4
12	452.0	180.7	150.0	124.9	20.1	6587.8
13	448.0	152.2	132.6	164.9	19.7	6470.0
14	404.0	130.0	118.4	151.9	15.6	5739.3
15	443.0	151.0	132.1	170.3	20.1	6528.8
16	464.0	157.5	135.9	175.7	21.5	6766.8
17	472.0	162.7	139.2	180.0	22.7	6961.9
18	429.0	144.8	127.7	164.5	18.6	6279.7
19	425.0	144.1	127.5	163.9	18.5	6258.9
20	519.0	174.1	147.5	180.0	24.8	9744.4
21	375.0	144.1	127.5	158.1	18.1	6170.6
22	503.0	174.1	147.5	180.0	24.8	9154.9
23	507.0	194.5	150.0	180.0	27.5	7622.8
24	490.0	179.7	150.0	180.0	25.7	7391.0

$v^{P,min}$: min. velocity for particle m;
ω_m^k: inertia coefficient at k^{th} iteration for particle m;
$\omega^{P,max}$: max. inertia coefficient for particle m;
$\omega^{P,min}$: min. inertia coefficient for particle m;
d_1, d_2: Particle acceleration constants;
ρ_1, ρ_2: Uniformly distributed random numbers between [0,1];
$\epsilon_{m,i}^P$: The contribute output of n^{th} unit in the extreme individuals for particle m;
$\varrho_{m,i}^P$: The contribute output of n^{th} unit in the global extreme of population;

PSO uses the location and the velocity of the particles to evaluate them using a fitness function or so-called evaluation function. For each particle, the personal best (*pbest*) and the global best position (*gbest*) is identified. Furthermore, the velocity of each particle identified by its distance from (*pbest*) and (*gbest*), and by its current velocity. After each iteration, the new position is updated as per the velocity, until the iterations are exhausted. The efficiency of the PSO is shown with the help of the figure 9, which shows the *gbest* value for the first 1000 iterations performed to find economic dispatch value at the hour 1.

Figure 2 shows the coordination between the operational blocks of the proposed system. It includes all of the above discussed sections as building blocks. The flow of methodology starts with the load forecasting using CNN. Futhermore, the RES output is fetched from mathematical functions by providing them data about solar irradiance and ambient temperature to PV power model, and wind speed to the wind power model. The a part of predicted load demand is fulfilled by RES and LFTGUs are economically dispatched for the remaining part of load demand. Therefore, PSO is

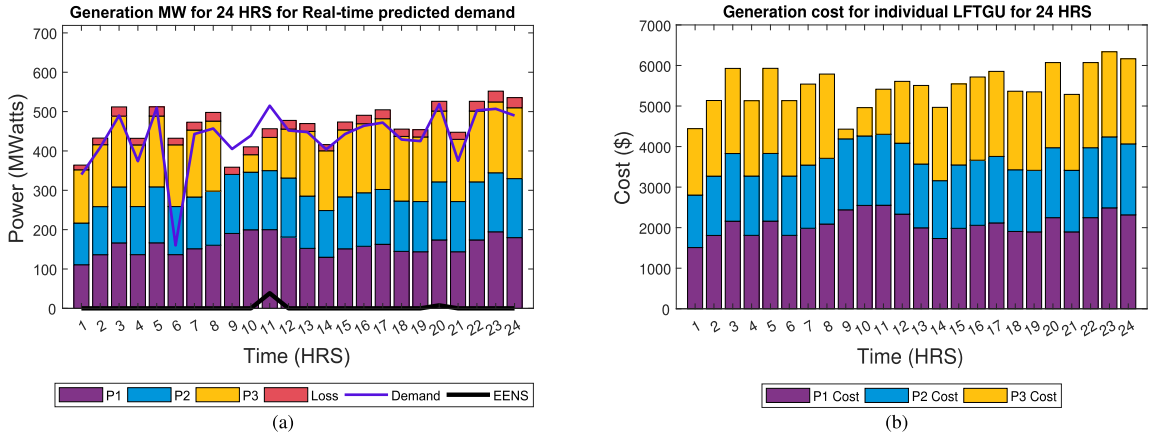

FIGURE 10. (a) Power generated by thermal units, (b) Generation cost for each LFTGU plotted for 24h.

used to get optimized results of the dispatch of LFTGUs, providing the IEEE standard data set of generators already used in our previous journal paper [31]. For instance, where LFTGUs, being dispatched within their operational limits, are not able to fulfill the total load demand, the BSS is involved in supplying the power. Hence, the BSS is implemented using simulink model presented in figure 5. At the instance where the supplied power becomes short and the load demand is not completely satisfied, the curtailed load is taken as EENS and it is penalized at a factor k^{VoLL}. On the other hand, the BSS is charged by supplying the surplus power when the dispatched power of LFTGUs is more than the load demand. In the same way, this flow is repeated to get results for 24 hours.

V. RESULTS

In this paper, the load forecasting results verified by comparing with a real time data of ISO-NECA, market data from January 2017 to December 2017, which has been taken from [17]. Hourly data of each day is considered, i.e., load demand is taken at 24 hourly instances in the day. CNN algorithm is applied within Python environment with Intel Core i3, 4GB RAM. The figure 8 gives the comparison of predicted results with the testing set of values.

The RES mathematical models are implemented in Matlab 2017. The wind model output is solely dependent on wind speed, which is taken for the 24 hourly instances in the day. Solar model incorporates the effect of solar irradiance and cell temperature on the power output of the PV panel. Moreover, the RES output power is shown in the figure 10d.

Thermal generating units used to supply the energy are dispatched for the amount of power demand not satisfied by using RES. The figure 10b gives the detailed profile of each generating unit taking part in the generated energy. The varying power demand is also displayed in 10b, presenting a slump in the demand on hour 6, caused by any fault on the transmission network. The generating units cannot adopt this drastic change in the production due to ramping, so the surplus power available is used to increase the SoC level of BSS. The table 5 shows the 24 hours cost to satisfy the

TABLE 6. EENS, SoC and RES.

Hours	EENS [MW]	SoC [%]	Power to BSS [MW]	PV output [MW]	Wind output [MW]
1	0.0	30.0	0.0	0.0	0.0
2	0.0	30.0	0.0	0.0	10.0
3	0.0	30.0	0.0	0.0	10.0
4	0.0	33.2	28.1	0.0	4.0
5	0.0	21.4	0.0	0.0	0.0
6	0.0	44.7	238.6	0.0	0.0
7	0.0	44.7	0.0	0.0	10.0
8	0.0	44.7	0.0	0.0	3.3
9	0.0	44.7	0.0	0.6	10.0
10	0.0	44.7	0.0	3.5	10.0
11	0.0	0.9	0.0	6.6	0.0
12	0.0	0.9	0.0	8.4	10.0
13	0.0	0.9	0.0	8.2	10.0
14	0.0	0.9	0.0	9.3	10.0
15	0.0	0.9	0.0	6.9	2.7
16	0.0	0.9	0.0	6.4	10.0
17	0.0	0.9	0.0	2.8	10.0
18	0.0	0.9	0.0	0.7	10.0
19	0.0	0.9	0.0	0.0	8.0
20	6.7	0.0	0.0	0.0	10.0
21	0.0	19.8	46.4	0.0	10.0
22	0.0	19.8	0.0	0.0	7.3
23	0.0	19.8	0.0	0.0	10.0
24	0.0	19.8	0.0	0.0	6.0

demand. The EENS is seen at the hour 9, which tells about the whole generation being short of the power demand. The total cost of running the generation units is given in the figure 7a. By running the optimal dispatch of thermal units, the cost calculated is the minimum possible value to satisfy the demand. This cost profile has shown a steep rise at the hour 9 which is due to the loss of generation unit in that time slot, as discussed in the test case 2. The power is produced at the remaining units which entails a rise in the cost of power generation. The VoLL is also plotted against the generation cost in the figure 7a. To get the individual cost contribution of each LFTGU, the 24 hours cost profile is shown in the figure 10c.

Furthermore, the surplus power available for the battery storage is shown in figure 7b. A large amount of surplus power is available in the hour 6, as there is a sudden fall

in the power demand due to fault occurred in the supply line, as described in the test case 1. Moreover, the SoC of BSS is shown in figure 7c. While, the table 6 shows the data regarding EENS. The data in EENS column gives details about the generating units not being able to fulfill the demand on the hour 20, so there is a part of load curtailed. The data in SoC column, demonstrates the case where the demand is low and generators are not able to reduce their generation due to ramping effect, the surplus power is sent to BSS which shows increase in SoC level as shown in hours 4, 6 and 21.

Despite the two troublesome occurrences in the test cases, the system has shown stability in terms of load demand satisfaction. In the instance where the loss of load is considered, the surplus power is used to be stored in BSS which will make the system stable without going towards power swings at the generation end. Furthermore, when one of the LFTGUs is taken out of the system, the short-fall in the generation will be covered by the BSS. In return, this will ease the remaining LFTGUs rather than getting under stress and facing power swings. The economic dispatch model is constrained in a way to operate well within their operational limits, i.e., not to lose their stability at any instance.

VI. CONCLUSION

In this paper, an economic dispatch for LFTGUs and BSS scheme with the integration of PV and wind power is proposed. The simulation results, comprise various profiles for 24 hours, are discussed in the results section. The demand is predicted from hourly data for a complete year. Two test cases are implemented during the simulation. At first instance, it is assumed that there is a sudden drop in the load demand caused by a failure in the distribution system. This catastrophic situation affects the generation end, but due to ramping, the LFTGUs are assumed not to undergo a sudden change in generated power, so the surplus power produced is available to be transferred to the BSS incorporated as a Simulink block. This phenomenon completes the test scenario experienced by the system. Then at another interval, one of the LFTGUs is assumed to confront an outage, and require minor maintenance. And the available generated power has fallen short of demanded power. Before the availability of the absent LFTGU, the leftover demand is attempted to be satisfied from BSS. Our proposed model shows the cost profile of our system not being majorly affected in both of the calamitous test cases.

ACKNOWLEDGMENT

The content of this [report/study/article/publication] does not reflect the official opinion of the European Union. Responsibility for the information and views expressed herein lies entirely with the author(s).

REFERENCES

[1] Y. Huang, J. Zhang, Y. Mo, S. Lu, and J. Ma, "A hybrid optimization approach for residential energy management," *IEEE Access*, vol. 8, pp. 225201–225209, 2020.

[2] S. A. Alhashmi, A. S. Al-Sumaiti, M. W. Hassan, M. B. Rasheed, S. R. R. Rodriguez, R. Kumar, and E. Heydarian-Forushani, "Building energy management system: An overview of recent literature research," in *Proc. Adv. Sci. Eng. Technol. Int. Conf. (ASET)*, Mar. 2019, pp. 1–5.

[3] T. M. Hansen, E. K. P. Chong, S. Suryanarayanan, A. A. Maciejewski, and H. J. Siegel, "A partially observable Markov decision process approach to residential home energy management," *IEEE Trans. Smart Grid*, vol. 9, no. 2, pp. 1271–1281, Mar. 2018.

[4] S. Althaher, P. Mancarella, and J. Mutale, "Automated demand response from home energy management system under dynamic pricing and power and comfort constraints," *IEEE Trans. Smart Grid*, vol. 6, no. 4, pp. 1874–1883, Jul. 2015.

[5] M. F. Balli, S. Uludag, A. A. Selcuk, and B. Tavli, "Distributed multi-unit privacy assured bidding (PAB) for smart grid demand response programs," *IEEE Trans. Smart Grid*, vol. 9, no. 5, pp. 4119–4127, Sep. 2018.

[6] A. Nawaz, G. Hafeez, I. Khan, K. U. Jan, H. Li, S. A. Khan, and Z. Wadud, "An intelligent integrated approach for efficient demand side management with forecaster and advanced metering infrastructure frameworks in smart grid," *IEEE Access*, vol. 8, pp. 132551–132581, 2020.

[7] E. S. Parizy, H. R. Bahrami, and S. Choi, "A low complexity and secure demand response technique for peak load reduction," *IEEE Trans. Smart Grid*, vol. 10, no. 3, pp. 3259–3268, May 2019.

[8] Z. Zhu, J. Tang, S. Lambotharan, W. H. Chin, and Z. Fan, "An integer linear programming and game theory based optimization for demand-side management in smart grid," in *Proc. IEEE GLOBECOM Workshops (GC Wkshps)*, Dec. 2011, pp. 1205–1210.

[9] A.-H. Mohsenian-Rad, V. W. S. Wong, J. Jatskevich, R. Schober, and A. Leon-Garcia, "Autonomous demand-side management based on game-theoretic energy consumption scheduling for the future smart grid," *IEEE Trans. Smart Grid*, vol. 1, no. 3, pp. 320–331, Dec. 2010.

[10] M. Pipattanasomporn, M. Kuzlu, and S. Rahman, "An algorithm for intelligent home energy management and demand response analysis," *IEEE Trans. Smart Grid*, vol. 3, no. 4, pp. 2166–2173, Dec. 2012.

[11] B. Yener, A. K. Erenoğlu, I. Şengör, O. Erdinç, A. Taşccıkaraoğlu, and J. P. S. Catalão, "Development of a smart thermostat controller for direct load control based demand response applications," in *Proc. Int. Conf. Smart Energy Syst. Technol. (SEST)*, Sep. 2019, pp. 1–5.

[12] C. Mao, F. Leng, J. Li, S. Zhang, L. Zhang, R. Mo, D. Wang, J. Zeng, X. Chen, R. An, and Y. Zhao, "A 400-V/50-kVA digital–physical hybrid real-time simulation platform for power systems," *IEEE Trans. Ind. Electron.*, vol. 65, no. 5, pp. 3666–3676, May 2018.

[13] N. T. Mbungu, R. C. Bansal, and R. Naidoo, "Smart energy coordination of a hybrid wind/PV with battery storage connected to grid," *J. Eng.*, vol. 2019, no. 18, pp. 5109–5113, Jul. 2019.

[14] A. Santhosh, A. M. Farid, and K. Youcef-Toumi, "Real-time economic dispatch for the supply side of the energy-water nexus," *Appl. Energy*, vol. 122, pp. 42–52, Jun. 2014.

[15] M. Bashari and A. Rahimi-Kian, "Forecasting electric load by aggregating meteorological and history-based deep learning modules," in *Proc. IEEE Power Energy Soc. Gen. Meeting (PESGM)*, Aug. 2020, pp. 1–5.

[16] H. Jahangir, H. Tayarani, S. S. Gougheri, M. A. Golkar, A. Ahmadian, and A. Elkamel, "Deep learning-based forecasting approach in smart grids with micro-clustering and bi-directional LSTM network," *IEEE Trans. Ind. Electron.*, early access, Jul. 21, 2020, doi: 10.1109/TIE.2020.3009604.

[17] S. Mujeeb, N. Javaid, M. Ilahi, Z. Wadud, F. Ishmanov, and M. Afzal, "Deep long short-term memory: A new price and load forecasting scheme for big data in smart cities," *Sustainability*, vol. 11, no. 4, p. 987, Feb. 2019.

[18] A. Ahmad, N. Javaid, A. Mateen, M. Awais, and Z. A. Khan, "Short-term load forecasting in smart grids: An intelligent modular approach," *Energies*, vol. 12, no. 1, p. 164, Jan. 2019.

[19] X. Shen, J. Liu, and H. Ruan, "A distributionally robust optimization model for the decomposition of contract electricity considering uncertainty of wind power," in *Proc. IEEE Int. Conf. Autom., Electron. Electr. Eng. (AUTEEE)*, Nov. 2018, pp. 64–68.

[20] Q. Xu, Y. Ding, and A. Zheng, "An optimal dispatch model of wind-integrated power system considering demand response and reliability," *Sustainability*, vol. 9, no. 5, p. 758, May 2017.

[21] Y.-S. Huang, J.-J. Deng, and Y.-Y. Zhang, "Application of SVM based on immune genetic fuzzy clustering algorithm to short-term load forecasting," in *Proc. Int. Conf. Mach. Learn. Cybern.*, Jul. 2008, pp. 2646–2650.

[22] F. L. Quilumba, W.-J. Lee, H. Huang, D. Y. Wang, and R. L. Szabados, "Using smart meter data to improve the accuracy of intraday load forecasting considering customer behavior similarities," *IEEE Trans. Smart Grid*, vol. 6, no. 2, pp. 911–918, Mar. 2015.

[23] W. Kong, Z. Y. Dong, D. J. Hill, F. Luo, and Y. Xu, "Short-term residential load forecasting based on resident behaviour learning," *IEEE Trans. Power Syst.*, vol. 33, no. 1, pp. 1087–1088, Jan. 2018.
[24] X. Fu, X.-J. Zeng, P. Feng, and X. Cai, "Clustering-based short-term load forecasting for residential electricity under the increasing-block pricing tariffs in China," *Energy*, vol. 165, pp. 76–89, Dec. 2018.
[25] V. Dvorkin, S. Delikaraoglou, and J. M. Morales, "Setting reserve requirements to approximate the efficiency of the stochastic dispatch," *IEEE Trans. Power Syst.*, vol. 34, no. 2, pp. 1524–1536, Mar. 2019.
[26] Z. Wu, J. Ding, Q. Wu, Z. Jing, and J. Zheng, "Reserve constrained dynamic economic dispatch with valve-point effect: A two-stage mixed integer linear programming approach," *CSEE J. Power Energy Syst.*, vol. 3, no. 2, pp. 203–211, Jul. 2017.
[27] S. Surender Reddy, P. R. Bijwe, and A. R. Abhyankar, "Real-time economic dispatch considering renewable power generation variability and uncertainty over scheduling period," *IEEE Syst. J.*, vol. 9, no. 4, pp. 1440–1451, Dec. 2015.
[28] S. S. Reddy and P. R. Bijwe, "Real time economic dispatch considering renewable energy resources," *Renew. Energy*, vol. 83, pp. 1215–1226, Nov. 2015.
[29] S. S. Reddy, "Optimization of renewable energy resources in hybrid energy systems," *J. Green Eng.*, vol. 7, nos. 1–2, pp. 43–60, 2017.
[30] M. Khoshjahan, P. Dehghanian, M. Moeini-Aghtaie, and M. Fotuhi-Firuzabad, "Harnessing ramp capability of spinning reserve services for enhanced power grid flexibility," *IEEE Trans. Ind. Appl.*, vol. 55, no. 6, pp. 7103–7112, Nov. 2019.
[31] M. Hassan, M. Rasheed, N. Javaid, W. Nazar, and M. Akmal, "Co-optimization of energy and reserve capacity considering renewable energy unit with uncertainty," *Energies*, vol. 11, no. 10, p. 2833, Oct. 2018.
[32] J. Contreras, M. Asensio, P. M. de Quevedo, G. Muñoz-Delgado, and S. Montoya-Bueno, "Renewable power generation models," in *Joint RES and Distribution Network Expansion Planning Under a Demand Response Framework*, J. Contreras, M. Asensio, P. M. de Quevedo, G. Muñoz-Delgado, and S. Montoya-Bueno, Eds. New York, NY, USA: Academic, 2016, ch. 2, pp. 7–19. [Online]. Available: https://www.sciencedirect.com/science/article/pii/B9780128053225000022
[33] V. Kornsiriluk, "Study of energy storage system: Concept of using ESS in EV charging stations in MEA," in *Proc. IEEE PES GTD Grand Int. Conf. Expo. Asia (GTD Asia)*, Mar. 2019, pp. 697–700.
[34] L. Chandra and S. Chanana, "Energy management of smart homes with energy storage, rooftop PV and electric vehicle," in *Proc. IEEE Int. Students' Conf. Electr., Electron. Comput. Sci. (SCEECS)*, Feb. 2018, pp. 1–6.
[35] P. S. Subudhi, K. Subramanian, and B. B. J. D. Retnam, "Wireless electric vehicle battery-charging system for solar-powered residential applications," *Int. J. Power Energy Syst.*, vol. 39, no. 3, pp. 130–140, 2019.
[36] P. S. Subudhi and S. Krithiga, "Wireless power transfer topologies used for static and dynamic charging of EV battery: A review," *Int. J. Emerg. Electr. Power Syst.*, vol. 21, no. 1, 2020, doi: 10.1515/ijeeps-2019-0151.
[37] A. Singh, S. Bhowmick, and K. Shukla, "Load compensation with DSTATCOM and BESS," in *Proc. IEEE 5th India Int. Conf. Power Electron. (IICPE)*, Dec. 2012, pp. 1–6.
[38] D. N. Rathod and A. P. Thakare, "Simulation for the most favorable competence of the BESS for the wind mills," in *Proc. Int. Conf. Comput., Commun., Control Autom. (ICCUBEA)*, Aug. 2017, pp. 1–5.
[39] N. Eghtedarpour and E. Farjah, "Distributed charge/discharge control of energy storages in a renewable-energy-based DC micro-grid," *IET Renew. Power Gener.*, vol. 8, no. 1, pp. 45–57, Jan. 2014.
[40] H. Shen, J. Liu, and L. Fu, "Self-learning Monte Carlo with deep neural networks," *Phys. Rev. B, Condens. Matter*, vol. 97, no. 20, May 2018, Art. no. 205140.
[41] J. Mitra, "Reliability-based sizing of backup storage," *IEEE Trans. Power Syst.*, vol. 25, no. 2, pp. 1198–1199, May 2010.
[42] J. Kumar, C. Parthasarathy, M. Västi, H. Laaksonen, M. Shafie-Khah, and K. Kauhaniemi, "Sizing and allocation of battery energy storage systems in åland islands for large-scale integration of renewables and electric ferry charging stations," *Energies*, vol. 13, no. 2, p. 317, Jan. 2020.
[43] Y. C. Hsieh, C. S. Moo, I. S. Tsai, and J. C. Cheng, "Dynamic charge equalization for series-connected batteries," in *Proc. IEEE Int. Conf. Ind. Technol. (ICIT)*, vol. 1, Dec. 2002, pp. 444–449.
[44] D. Mazzeo, G. Oliveti, C. Baglivo, and P. M. Congedo, "Energy reliability-constrained method for the multi-objective optimization of a photovoltaic-wind hybrid system with battery storage," *Energy*, vol. 156, pp. 688–708, Aug. 2018.

M. WAJAHAT HASSAN received the M.S. degree in electronics and electrical systems with a focus on electrical power system optimization from The University of Lahore. He is currently an Assistant Professor with The University of Lahore, Pakistan. He has demonstrated a history of working in the education management industry and is skilled in electrical power flow optimization, machine learning using Python language.

THAMER ALQUTHAMI received the Ph.D. degree in electrical engineering (mathematics) from the Georgia Institute of Technology. He is an experienced Assistant Professor with a demonstrated history of working in higher education and industry. His skills include PSCAD/EMTDC, Python, PTI/PSSE, RTDs, Building Automation Implementation, R-Statistics, and C++. His research interests include smart grids, renewable energy, power system operation and control, complex system modeling and simulation, energy audit, energy efficiency and savings, and data analytics.

AHMAD H. MILYANI received the B.Sc. (Hons.) and M.Sc. degrees in electrical and computer engineering from Purdue University, in 2011 and 2013, respectively, and the Ph.D. degree in electrical engineering from the University of Washington, in 2019. He is currently an Assistant Professor with the Department of Electrical and Computer Engineering, King Abdulaziz University, Jeddah, Saudi Arabia. His research interests include power systems operation and optimization, renewable and sustainable energy, power electronics, electric vehicles, and machine learning.

ASHFAQ AHMAD received the M.S. degree in power engineering from The University of Lahore, Lahore, Pakistan, in 2011, and the Ph.D. degree from the University of Science and Technology of China, China, in 2020. He is currently working as an Associate Professor with the Department of Electronics and Electrical Systems, The University of Lahore. His research interests include power engineering, power transmission system modelling and, photovoltaic power system modeling using artificial intelligent machine learning methods.

MUHAMMAD BABAR RASHEED (Senior Member, IEEE) received the master's and Ph.D. degrees from COMSATS University Islamabad, in 2013 and 2017, respectively. He obtained postdoctoral fellowships from Durham University, U.K., and King Abdulaziz University (KAU), Saudi Arabia, in 2019 and 2020. He is currently working as a GET-COFUND Marie Curie Fellow with UAH, Spain. Previously, he was serving as an Associate and Assistant Professor with the Department of Electronics and Electrical Systems, The University of Lahore, Pakistan. He has authored over 40 peer-reviewed articles in well-reputed journals and conference proceedings and supervised more than ten students in their final year projects and thesis. His research interests include LP, NLP, and heuristic optimizations, machine learning, smart grids, electric vehicles, and demand response. He is an Active Reviewer of many esteemed journals and conferences, including IEEE Transactions, IEEE Access, IEEE Transactions on Industry Application Systems, *Applied Energy*, and *Energies*.